

# Adaptive Sampling of Surface Fronts in the Arctic Using an Autonomous Underwater Vehicle

Trygve Olav Fossum , Petter Norgren , Ilker Fer , Frank Nilsen, Zoe Charlotte Koenig, *Member, IEEE*, and Martin Ludvigsen 

**Abstract**—Fronts between Arctic- and Atlantic-origin waters are characterized by strong lateral gradients in temperature and salinity. Ocean processes associated with fronts are complex with considerable space and time variability. Therefore, resolving the processes in frontal zones by observation is challenging but important for understanding the associated physical–biological interactions and their impact on the marine ecosystem. The use of autonomous robotic vehicles and *in situ* data-driven sampling can help improve and augment the traditional sampling practices, such as ships and profiling instruments. Here, we present the development and results of using an autonomous agent for detection and sampling of an Arctic front, integrated on board an autonomous underwater vehicle. The agent is based on a subsumption architecture implemented as behaviors in a finite-state machine. Once a front is detected, the front tracking behavior uses observations to continuously adapt the path of the vehicle to perform transects across the front interface. Following successful sea trials in the Trondheimsfjord, the front-tracking agent was deployed to perform a full-scale mission near 82°N north of Svalbard, close to the sea ice edge. The agent was able to detect and track an Arctic frontal feature, performing a total of six crossings while collecting vertical profiles in the upper 90 m of the water column. Measurements yield a detailed volumetric description of the frontal feature with high resolution along the frontal zone, augmenting ship-based sampling that was run in parallel.

**Index Terms**—Adaptive sampling, Arctic, autonomous under water vehicle (AUV), data-driven sampling, fronts.

Manuscript received September 11, 2019; revised November 12, 2020; accepted March 26, 2021. Date of publication June 2, 2021; date of current version October 13, 2021. This work was supported in part by the Nansen Legacy Program ([www.arvenetternansen.com](http://www.arvenetternansen.com)) under Project 276730, and in part by the AMOS ([www.ntnu.edu/amos](http://www.ntnu.edu/amos)) Center of Excellence, under Project 223254. (Corresponding author: Trygve Olav Fossum.)

**Associate Editor:** N. Cruz.

Trygve Olav Fossum and Petter Norgren are with the Department of Marine Technology, Norwegian University of Science and Technology (NTNU), 7491 Trondheim, Norway, and also with the Centre for Autonomous Marine Operations and Systems (AMOS), 7491 Trondheim, Norway (e-mail: trygve.o.fossum@ntnu.no; petter.norgren@ntnu.no).

Ilker Fer and Frank Nilsen are with the Geophysical Institute, University of Bergen and Bjerknes Centre for Climate Research, 5007 Bergen, Norway, and also with The University Centre in Svalbard (UNIS), 9171 Longyearbyen, Norway (e-mail: Ilker.Fer@uib.no; Frank.Nilsen@unis.no).

Zoe Charlotte Koenig is with the Geophysical Institute, University of Bergen and Bjerknes Centre for Climate Research, 5007 Bergen, Norway, and also with the Norwegian Polar Institute, 9296 Tromsø, Norway (e-mail: zoe.koenig@uib.no).

Martin Ludvigsen is with the Department of Marine Technology, Norwegian University of Science and Technology (NTNU), 7491 Trondheim, Norway, with the Centre for Autonomous Marine Operations and Systems (AMOS), 7491 Trondheim, Norway, and also with The University Centre in Svalbard (UNIS), 9171 Longyearbyen, Norway (e-mail: martin.ludvigsen@ntnu.no).

Digital Object Identifier 10.1109/JOE.2021.3070912

## I. INTRODUCTION

OCEANIC fronts are dynamic boundaries where different water masses meet and interact. Large changes in water properties (such as temperature, salinity, or dissolved oxygen concentration) result in elevated horizontal gradients that can be used to detect their presence. Ocean ecosystems thrive in fronts [1], which are typically associated with enhanced primary production [2], [3], high concentrations of zooplankton and fish larvae [4], and biogeochemical cycling [3]. Flow convergence along fronts also induces patchiness, vertical mixing, and increased nutrient supply [5].

The observational practices of frontal processes are usually scale dependent, as different frontal processes occur across a variety of spatial scales [from 1–10 km (*submesoscale*) up to 50 km (*mesoscale*)] and directions (along-front and cross-frontal process scales) [6]; propagating vortices, frontal meandering, and ocean turbulent patchiness further introduce temporal variability. Therefore, a lack of resolution in time or space can fail to capture important dynamics and their variability. Traditional ocean sensing practices, such as profiling at stations occupied by a ship, or transects using sensors towed behind a vessel, impose both economic and logistical limitations that compromise the spatial and temporal coverage of the observations. Satellite imagery from polar orbiting satellites has been extensively used to observe ocean surface fronts; see, e.g., [7]. As there is an inherent latency between capture and availability, surface coverage only, cloud dependence, combined with the tidal movements and ocean dynamics, the use of satellite-based remote sensing disallow direct use in resolving subsurface details and tracking the front. Thus, a sustained focus on effective use and consolidation of sampling resources and acquisition strategies has consequently emerged [8]–[11]. As a result of these developments, the use of robotic assets has increased, providing mobility and adaptive sampling capabilities that can substantially augment current ocean observation practices.

Autonomous underwater vehicles (AUVs) are effective for observing submesoscale features such as fronts, and have been used in numerous water-column sampling applications [8], [11]–[13] and field programs. For instance, the Autonomous Ocean Sampling Network (AOSN-I/II) [14], [15] conducted a study to understand how ocean variability could be observed using a coordinated network of assets. Central to the success of these efforts were decentralized *adaptive sampling* strategies running locally on board the sensing platforms. Such sampling is capable

of adjusting the mission execution according to the evolving dynamics of a feature—such as a front or a coherent vortex—without human intervention.

Polar regions, particularly in the marginal ice zone, are characterized by strong lateral gradients in water mass properties in the upper water column. In the region north of Svalbard, the warm and saline Atlantic Water (AW) flows into the Arctic Ocean as a boundary current leading to open (sometimes fragmented), ice-free waters in the region. This has consequences for the marine ecosystem, regional air–ice–sea interaction processes and, thus, vertical mixing and ocean circulation [16]. The high-latitude regions are also challenging environments for AUV operations due the presence of drifting sea ice and a harsh climate (low temperatures and strong winds) impacting deployment and recovery operations. The lack of over-the-horizon communication infrastructure (often limited to satellite only) also increases complexity and requirements for these systems to be self-reliant. The remote and isolated locations imply that the time available for sampling is highly valuable and must be used efficiently. Autonomous assets have the potential to contribute to data collection and knowledge generation by delivering target-specific and intelligent sampling schemes, which aim to resolve processes and scales of interest.

Using an AUV equipped with a CTD (i.e., conductivity, temperature, depth) sensor and water quality sensors (more details in Section IV-A), we have developed and tested a sampling algorithm for detection, tracking, and mapping of a polar front. The aim of the algorithm is twofold: 1) automatically detect and track the front based on the horizontal gradient of temperature; and 2) refine and increase the sampling resolution both along the front and sufficiently into the water masses on either side of the front. The AUV was deployed and recovered during the Nansen Legacy cruise on *R/V Kronprins Haakon* in September 2018, from which CTD profiles were collected in parallel during the AUV operation. An overview of the experiment setup and involved systems are shown in Fig. 1(a), together with the deployment location relative to Svalbard [see Fig. 1(b)].

## II. RELATED WORK

Autonomous and adaptive feature tracking of frontal features was explored for a horizontal (i.e., 2-D) single-location (across-front sampling) upwelling system in [12] using the horizontal temperature gradient in a stratified water column, where the vertical temperature difference is large between stratified layers compared to upwelling (mixed) water. The method was successfully used to map an upwelling frontal system in Monterey Bay, CA, USA, April 2011, completing 14 transects across the front. The method was later extended to accommodate along-front tracking in [17] for deployment on board an unmanned surface vehicle. Building on this, as well as related experiments in [18] and [19] developed a method for both across- and along-front tracking capable of both 2-D and 3-D tracking. The method was tested in a virtual environment using ocean model data. An adaptive path planning algorithm for 2-D tracking of ocean fronts was also presented in [13], based on adjusting a cubic spline from a set of predefined assumptions about the properties

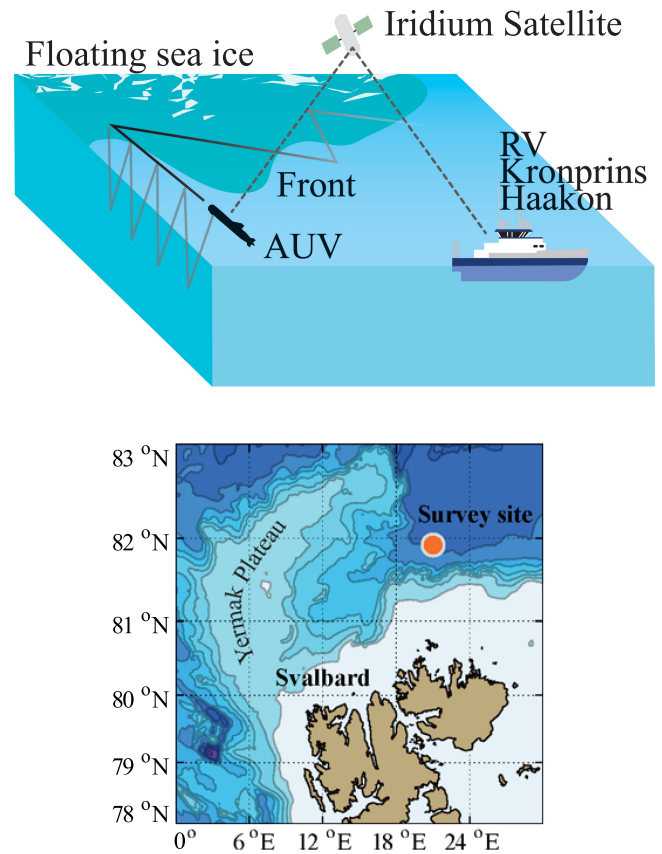


Fig. 1. (a) Illustration of the experiment setup north of Svalbard showing the ship, satellite, and the AUV crossing the front between warm (light blue) and cold (dark blue) waters close to the ice edge (white). (b) Map showing the location of the experiment relative to Svalbard. Isobaths are at 500-m intervals.

of a front. A zigzag pattern was then derived based on the adjusted curve to cover the across-front variation. The method was restricted to tracking only, but could not find or relocate the front. In [20], an adaptive sampling and tracking algorithm of a near-shore frontal feature (a river plume) was explored outside Porto, Portugal using a state-based autonomous agent on board an AUV that performs tracking on a threshold detection of salinity (isopycnal) and state switching. As the method was developed for a disc-shaped river plume, a constant angle increment was used to traverse the disk feature. Other related work on reactive tracking of thermocline features using AUVs includes [21]–[23]; each describe the procedure and results of tracking the vertical temperature gradient in the water column using a state machine with different behaviors that issues depth specific set-points [in each case, adaptation only occurs in the  $z$ -direction, one-dimensional tracking]. An important aspect for all front tracking is to keep contact with the boundary feature. In [24], this is addressed by adapting the orientation of the crossings to the local curvature of the boundary. When available, multivehicle approaches are able to resolve spatial features more effectively and in turn provide an enhanced synopticity of the frontal boundary, as demonstrated in, e.g., [25], where several platforms were coordinated to sample an upwelling front in Monterey Bay.



where  $n_d$  is the number of measurements inside the depth interval, and  $t_d$  the associated temperatures. To determine the position to the AUV relative to the front, we define a variable  $s_{\text{front}}$  that can take on the values  $s_{\text{front}} = \text{inside}$  or  $s_{\text{front}} = \text{outside}$ . We also define a variable  $\tilde{s}_{\text{front}}$  as follows:

where  $T_{\text{isotherm}}$  is the constant defining the frontal isotherm and  $T_{\text{hysteresis}}$  is the constant defining the hysteresis sensitivity. A frontal crossing is confirmed if  $s_{\text{front}} \neq \tilde{s}_{\text{front}}$  for two consecutive yoyo envelopes, in which case  $s_{\text{front}}$  changes from *inside*  $\rightarrow$  *outside* or from *outside*  $\rightarrow$  *inside*.

### III. METHOD

The method is based on a finite-state machine (FSM) following classical reactive subsumption-based approaches [26]. The main idea is to generate a zigzag maneuver triggered by a switch between two main descriptive states dependent on the AUV location relative to the front (inside/outside). As the front is partially due to melt water (with low density), the strongest frontal signature is near the surface; hence, only measurements from a predefined depth interval (0.5–8 m) are used for detection. For the surface fronts discussed here, this depth interval can be a fixed constant or be adapted based on experience. We define the average temperature from the depth interval as

### 1) Step-by-Step Description of the FSM:

- Authorized licensed use limited to: Norges Teknisk-Naturvitenskapelige Universitet. Downloaded on January 28, 2022 at 15:15:24 UTC from IEEE Xplore. Restrictions apply.



- 1) Perform steps a)–c) of *search mode*.
- 2) If detection counter is greater than 2:
  - a) increase the front crossing counter;
  - b) switch the current state  $s_{\text{front}}$ : *inside*  $\rightarrow$  *outside* or *outside*  $\rightarrow$  *inside*;
  - c) generate new zigzag maneuver.
- 3) If maximum number of front crossings is reached, switch state to *return* using predefined home waypoint.
- 4) If end is reached without a front is detected, switch state to *recover front*:
  - a) change state to *recover front*;
  - b) generate new regain maneuver.
- 3) *Recover front mode*—Attempt to recover front using regain maneuver.
  - a) Perform steps a)–c) of *search mode*.
  - b) If the detection counter is greater than 2:
    - i) change state to *track front*;
    - ii) generate new zigzag maneuver;
  - 3) If end is reached without front detection:
    - a) if regain attempts is less than maximum, generate new regain maneuver;
    - b) else, switch state to *return* using predefined home waypoint.

2) *Description of Zigzag and Regain Maneuvers*: Fig. 2 also presents insight into the generation of the zigzag maneuver, as well as the maneuver used to regain the front if it is lost. The predetermined zigzag patterns assume that the front is approximately orthogonal to the heading when detection [which has to be verified twice (Det. 1 and Det. 2 in the figure)] was made. This requires using a *turn angle* (set to  $45^\circ$ ) and a predetermined *step in*, which allows the pattern to steer toward another crossing of the front. A *step out* is also taken initially after detection to sample well within the different sides of the front.

Finally, the *regain* maneuver is an important addition to the tracking behavior, allowing the AUV to regain the front; this is important if the curvature of the front is high, as a fixed angle zigzag maneuver will have difficulties following the front boundary. The maneuver is initiated after a completed zigzag maneuver without any front detection. The essence is to back-track to the place where the front was last detected and approaches this point with a different heading. The maneuver uses a predefined *backtrack-step*, and *regain-step* (shown in red text in Fig. 2) sets to be half the length of the *step-in* distance. Execution of the *backtrack-step* is followed by a  $90^\circ$  turn angle, before the *regain-step*, resulting in a path that ends where the last front crossing was detected. This maneuver can also be run multiple times if necessary (see, e.g., Fig 3). Continuing to run the maneuver will cause the AUV to loiter around in a square pattern (due to the regain back-tracking step) until a certain number of repetitions have been made (five in our case), at which point the AUV returns to a predetermined home location.

### B. Sea Trial in the Trondheimsfjord

Before the deployment in the Arctic, a field trial was made in the Trondheimsfjord using a simulated front. Measurements were fed to the sensor from a simulation engine that relied on

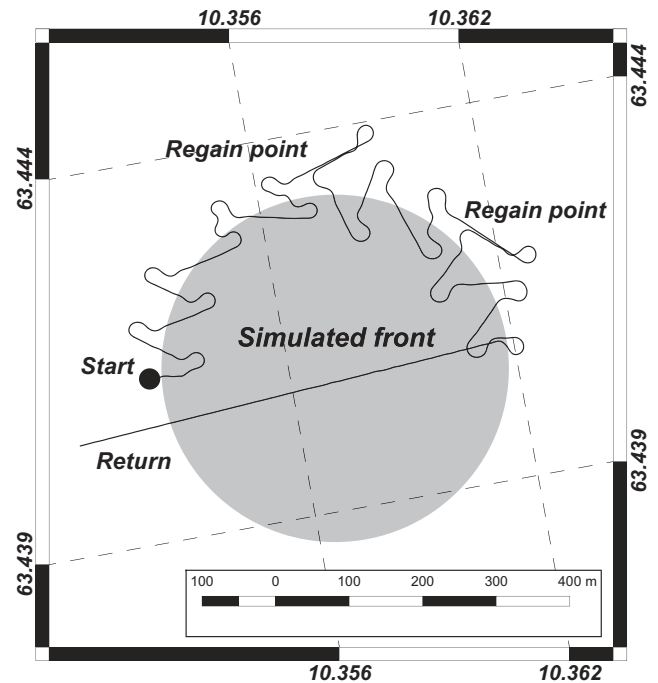


Fig. 3. AUV path in the Trondheimsfjord. The AUV tracks a simulated front using sensor spoofing, crossing the front, losing contact, and regaining contact using the *regain* maneuver.

calculating the radial distance from the AUV to a predetermined coordinate. If the AUV was within a given radius, shown in gray in Fig. 3, measurements would change to reflect that the AUV had crossed the front. The *zigzag* maneuver would then be triggered and the AUV would turn to cross the front once again. The simulated front was programmed to be circular with a radius of about 250 m and, hence, had a large curvature. The assumption that the heading would be orthogonal does not hold for a fixed turn angle, and thus, the AUV would eventually lose the front and would have to execute the *regain* maneuver. The resulting AUV track from the trial is shown as a black line in Fig. 3. As indicated, the AUV successfully navigated the simulated front, executing both the *zigzag* and *regain* maneuvers. The trial also shows that the AUV successfully regained track of the front after a failed detection attempt. Due to the small scale of the front, the  $45^\circ$  turns of the AUV can be seen clearly.

## IV. EXPERIMENTAL RESULTS

### A. Experiment Setup: LAUV Harald

The AUV platform used in our experiments was a 2.4-m-long, 100-m rated OceanScan Light AUV (LAUV) [27], capable of more than 24 h of in-water operation; see Fig. 4. The payload included a 16-Hz SeaBird FastCAT 49 CTD (conductivity, temperature, and depth) sensor; a WetLabs Triple-Measurement Meter EcoPuck, measuring color-dissolved organic matter at 370/460 nm, chlorophyll *a* fluorescence at 470/695 nm, and optical backscatter; and an Aanderaa 4831 optode for measuring dissolved oxygen concentration. The accuracy of the CTD instrument is  $\pm 0.0003 \text{ S} \cdot \text{m}^{-1}$  (conductivity) and  $\pm 0.002^\circ \text{C}$

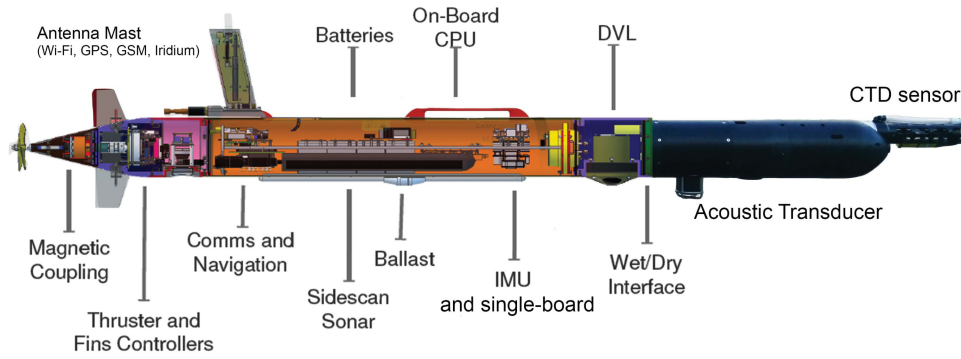


Fig. 4. AUV platform used in the experiment. Sensors and hardware components are shown as integrated.

(temperature); accuracy of the dissolved oxygen sensor is less than  $8 \mu\text{mol} \cdot \text{L}^{-1}$ . The chlorophyll *a* fluorescence sensor has a sensitivity of  $0.016 \mu\text{g} \cdot \text{L}^{-1}$  and the CDOM of 0.184 ppb.

The front tracking algorithm was hosted on an NVIDIA Jetson TX1 multicore single-board computer, running through the autonomous agent architecture T-REX (Teleo-Reactive Executive), and executing tasks continuously as sensing and control data are fed to it from the integrated control system, DUNE [28], [29].<sup>1</sup> Details of T-REX are beyond the scope of this work; readers are referred to [30] and [31] for more information.

#### B. Experiment at Svalbard—The Nansen Legacy Campaign

The front experiment was conducted north of Svalbard at approximately  $82^\circ\text{N}$  [see Fig. 1(b)], during cruise KH2018709 onboard *R/V Kronprins Haakon* (September 14–24, 2018). The AUV deployment was augmented by hydrographic profiles collected using the ship's CTD system (Sea-Bird Scientific, SBE 911plus). An overview of the experimental setup and involved systems is shown in Fig. 1(a). The ship maintained a safe distance from the AUV operation area during the survey to avoid interference and collision (the AUV is not visible by eye from the ship bridge). This distance dictated that only satellite communications could be used, making autonomy and adaptation strictly necessary.

The AUV was deployed on September 18, 2018, and three missions were made between 07:00 (start first mission) and 16:34 UTC (end last mission), with duration of 238, 112, and 56 min, respectively. Deployment and recovery were made using a light work boat. Of the three missions, the front was detected and tracked only in the first mission (238 min). The latter missions failed to find the front as the front had receded toward the ice edge, moving 4 km northward; this eventually prompted the commanded abort of the AUV less than 500 m from the ice edge in the last mission (56 min). Consequently, only the results from the first mission are presented. Here, the AUV successfully tracked the front along the predefined  $T_{\text{isotherm}} = 1.5^\circ\text{C}$  contour line. A detailed description of the mission parameters used by the FSM is given in Table I.

1) *AUV Data*: Fig. 5 shows the AUV path superimposed on a horizontal spatial interpolation of the temperature measurements from 0.5- to 8-m depths. The interpolation clearly marks the

TABLE I  
MISSION PARAMETERS

Parameter	Value	Comment
Step out	300 m	Travel after detection
Step in	2500 m	Distance to cross front
Turn angle	$45^\circ$	Turn angle
Detection temperature	$1.5 \pm 0.5^\circ\text{C}$	$T_{\text{isotherm}} \pm T_{\text{hysteresis}}$
Detection depth	0.5–8.0 m	The detection depth interval
Yoyo depths	0–90 m	Min and Max depths
Number of crossings	6	Front crossings

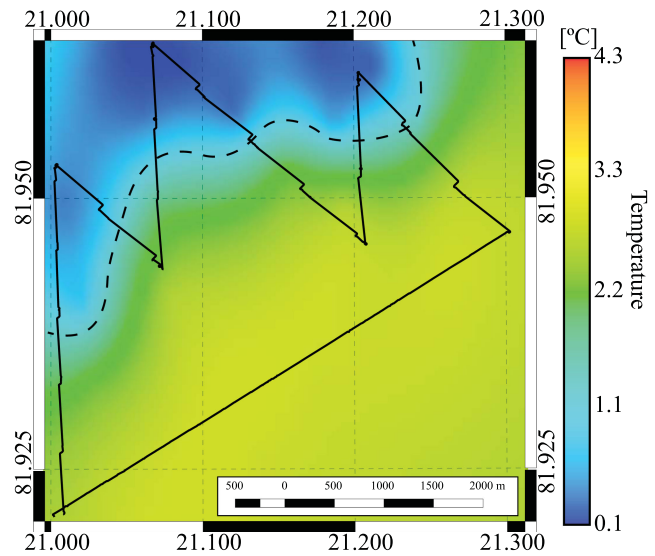


Fig. 5. Map of the AUV path overlaid on the 2-m cut plane from the interpolated (kriged) measurements, with the front indicated (dashed line).

front, which can be seen as the dashed line. A total of six crossings made during the first mission were conducted over 4 h (23 km), with a mean speed of 1.6 m/s. As designed, the AUV samples well within each water mass on both sides of the front while tracking the orientation of the front toward the northeast. The jagged AUV path is due to drift of the inertial navigation system, which resets upon surfacing (hence, the jump). A clear drift toward the southwest can be indicative of currents influencing the AUV in this direction. The AUV covered the water

<sup>1</sup>[Online]. Available: <http://lists.pt/toolchain>

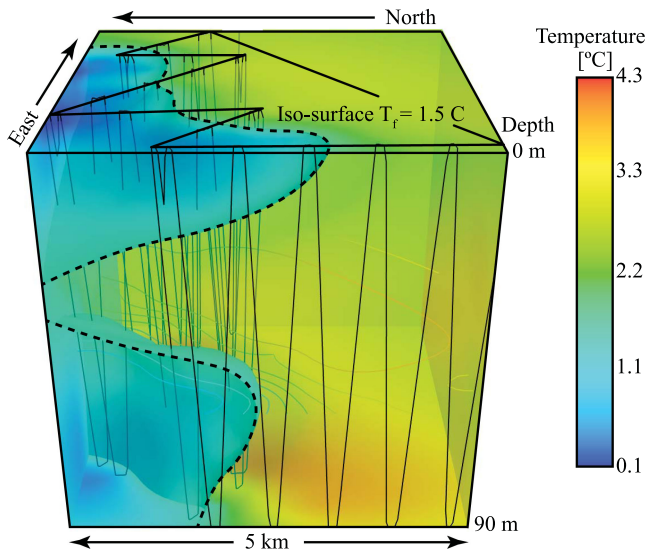


Fig. 6. Volumetric temperature distribution as estimated from kriging (see, e.g., [34]). The vertical saw-tooth pattern of the AUV path can be seen in black, crossing back and forth the warm/cold temperature front. Side view.

column from 0 to 90 m throughout the mission, except for the last northeast–southwest segment where the AUV returned back on the surface (as a safety precaution to keep contact).

By combining all the measurements from the AUV profiles (yoyo from 0 to 100 m), a volumetric representation of the front structure can be rendered. This can be seen in Fig. 6, which shows the estimated 3-D temperature distribution obtained using kriging [32] (where correlation parameters were adjusted for stratification, increasing the horizontal correlation) together with the AUV path. The temperature data were spatially averaged and discretized to a  $50 \times 50 \times 50$  cell volume grid. As the measurements were collected over a period of 4 h, the volumetric interpolation will not be accurate as a temporal snapshot. This time distortion can be improved by using Lagrangian measurement strategies or more complex correlation functions; see, e.g., [33]. The front is shown as an isosurface with its outline marked for clarification. The front has an intrusion of warm water at 40 m that arises from the frontal dynamics; this is further discussed in detail in [7].

**2) Comparison With Ship Data:** The AUV and shipboard measurements are not fully contemporaneous or colocated; hence, a detailed comparison or validation was not attempted. However, the near-surface measurements of the frontal region and the Atlantic and polar origin waters from the thermosalinograph of the ship are consistent with the AUV measurements (see Fig. 7). Using data points collected within 2 km and 2 h by the two platforms, average temperature measured by the AUV between 3- and 5-m depths, and from the thermosalinograph (water intake depth 4 m), root-mean-squared difference was  $0.07^\circ\text{C}$ , increasing from  $0.05^\circ\text{C}$  on the warm side to  $0.09^\circ\text{C}$  on the cold side. A comparison with the CTD profiles is not attempted because the distance to the nearest CTD station was larger than 2 km. When combined, the measurements obtained from the two platforms allow for a larger spatial coverage. The AUV,

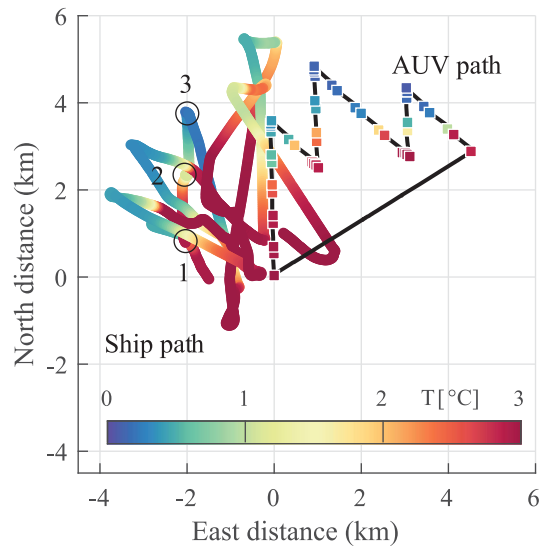


Fig. 7. Near-surface temperature measured by the ship's thermosalinograph (color coded) along the ship's track together with the AUV path (black). CTD stations 1 to 3 across the front are marked with black circles. Horizontal distance is referenced to the AUV deployment location.

therefore, substantially augments the sampling by performing an efficient track using the adaptive sampling method.

Without continuous profiling by an undulating towfish, an underwater glider, or an AUV as employed here, typical ship-board sampling would be conducted using the ship's CTD. We exemplify this using three CTD profiles collected from the ship (see Fig. 7, stars). They are spaced out on the warm side, at the front, and the cold side of the boundary. The profiles, down to 500-m depth, are shown in Fig. 8. Although a higher spatial resolution can be achieved by collecting shallower profiles, such measurements would compromise the much-needed deep hydrographic measurements during a cruise. An AUV, thus, provides high horizontal resolution in parallel to ship's operations, making this an attractive technology for process studies.

**3) Observations:** The profiles (see Fig. 8) reflect the complex structure of water masses found north of Svalbard that result from the different routes AW can take to reach this area. The different routes determine the water mass modification that AW experiences along its path. On the warm side of the front, between 50- and 250-m depths, we see nearly pure AW with a temperature above  $3^\circ\text{C}$  and salinity above 34.9, implying negligible dilution with surrounding waters. This suggests that these waters likely followed a short route across the Yermak Plateau [shown in Fig. 1(b)]. Modified AW with a reduced temperature is found below this depth on both sides of the front. Relatively diluted waters could represent water that has been modified along a longer route, e.g., around or across the Yermak Plateau. When warm AW meets and melts sea ice, a colder and relatively less saline water mass is formed in the surface layer. The melt water reduces the density in the upper layer, increases the vertical stratification, and can protect sea ice from further melting. The relatively fresh layer in the upper 50 m on the warm side can be associated with melting. However, the most

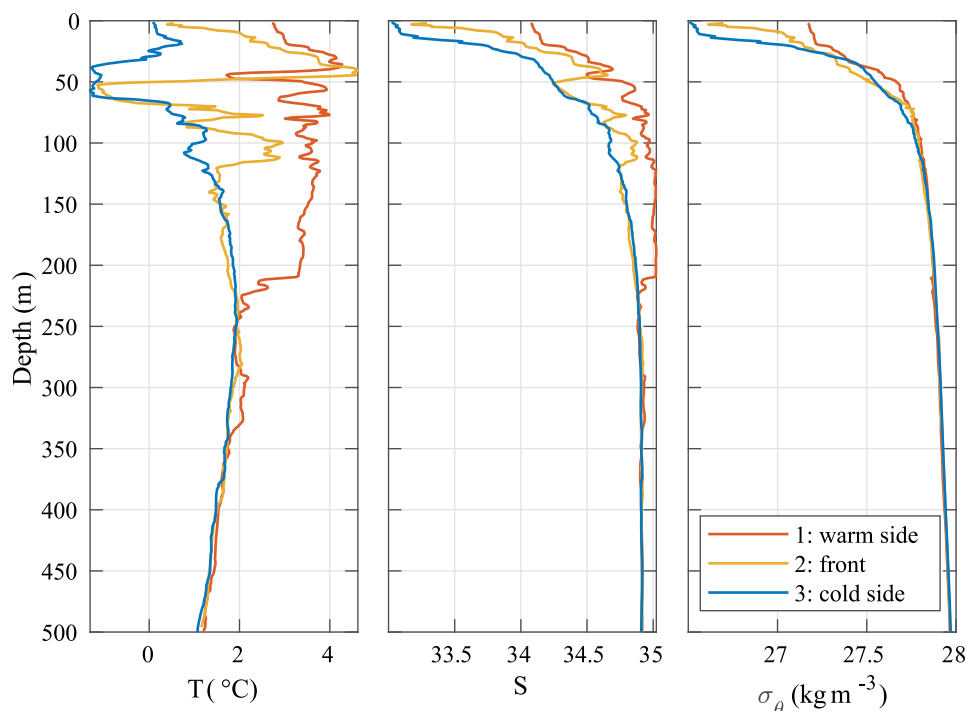


Fig. 8. Temperature, salinity, and potential density anomaly profiles collected at stations 1–3, in the warm side, at the front, and in the cold side of the front.

pronounced stratification on the cold side of the front with lowest upper layer salinity is the cold and fresh Polar Water that has been formed in the Arctic Ocean. The gradient from warm and saline AW toward the cold and less saline waters is notable, and generates the front sampled. However, the vertical structure of the gradients of temperature, salinity, and density between the warm and cold sides of the front is different. While the lateral density gradient is pronounced only in the upper 30 m, temperature and salinity profiles show large differences reaching as deep as 200 m.

The AUV, with its high spatial resolution, allowed for a detailed mapping of the across-front structure. Fig. 9 presents cross-front sections of the different parameters, with the warm side located at distance  $y < 0$  km and the cold side at  $y > 0$  km, where  $y$  is the cross-front distance in kilometers. Details about the construction of the sections can be found in [7]. The AUV mission was designed to cross the surface temperature front, but it also criss-crossed a deeper front. The front separates the warm and saline AW coming directly from Fram Strait from the colder and fresher Polar Water that has been formed in the Arctic Ocean. The front has a distinct signature in Chlorophyll a fluorescence, with larger concentrations on the warm side. A subsurface maximum of Chlorophyll a was found at about 30-m depth on the cold side. Northeasterly winds during the cruise forced the warm and dense mixed layer to downwell beneath the cold, lighter side, supported by current observations from a ship-mounted acoustic Doppler current profiler. At around 40-m depth, a warm intrusion is observed in Fig. 9, in close agreement with the intrusion captured at 50 m in the shipborne CTD profile at the front.

## V. DISCUSSION

For a subsumption architecture such as the one presented here (see Fig. 2), the sensory information couples directly with action selection, with a limited state-based model of the environment. There is no need for a complex internalized model as there is no planning or deliberation involved, but only actions in response to sensor values. Constructing a successful sampling approach rests upon the practicability of decomposing the problem into different sets of behaviors that represent certain action–response pairs that are triggered by the incoming data. The frontal structure studied is simple enough that this is possible. However, handling off-nominal endogenous or exogenous conditions, including the presence of multiple fronts, can result in complications as the potential growth of the number of states and the associated intelligent switching needed to resolve conflicts or priorities. Introduction of a more elaborate environmental model would alleviate the complexity of the FSM. A natural extension would then be a more deliberative hybrid system, where a state-based reasoning would only occur at the highest level, leaving more detailed planning to more information-theoretic approaches (see [35]).

In the FSM implementation shown here, prior information of the front dynamics, such as the estimated temperatures on each sides of the front, is necessary to define the hysteresis used for detection. This can be deduced automatically by having the AUV search for a gradient with a predefined magnitude instead, which would simplify the configuration of the FSM. One could also foresee an extension with more elaborate behaviors for keeping track of the frontal boundary (e.g., [21]). Additionally, an online estimate of the front dynamics could be deduced from



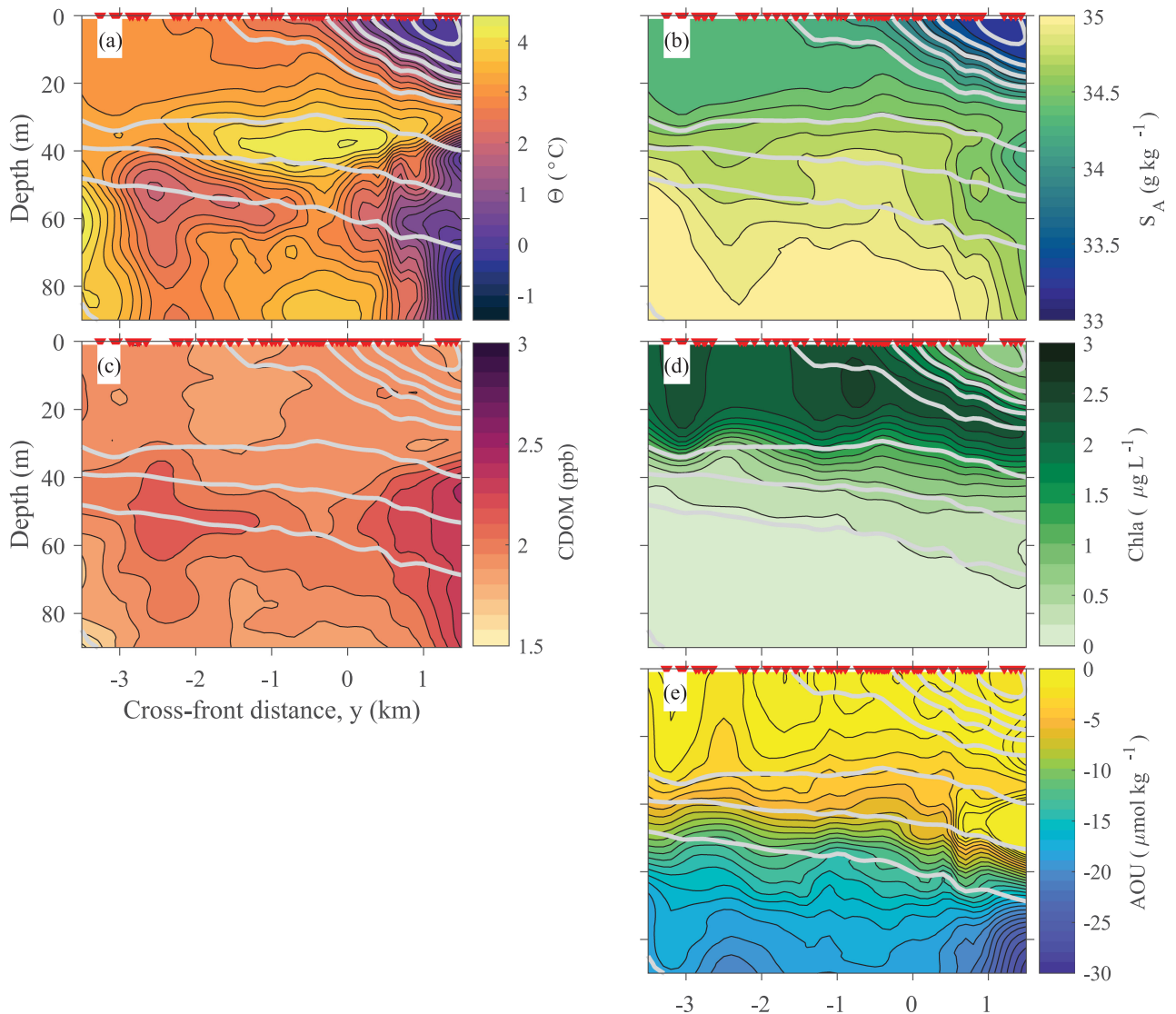


Fig. 9. Cross-front sections based on AUV data of (a) Conservative Temperature ( $\Theta$ ), (b) Absolute Salinity ( $S_A$ ), (c) CDOM (ppb), (d) chlorophyll *a* fluorescence, and (e) apparent oxygen utilization (AOU). The red triangles are the location of the AUV profiles. The gray lines are isopycnals (every  $0.1 \text{ kg} \cdot \text{m}^{-3}$ ).

either current measurements or more elaborate statistical models (see, e.g., [36]).

The spatial scales associated with oceanographic processes (fronts, eddies, etc.) are large (10–100 km) compared to the typical distance covered by short AUV missions. While a single transect can cover about 30 km in a 6-h mission at 1.5 m/s, multiple crossings of a feature will be limited in scale. However, targeted measurements such as those conducted here return high-resolution observations, which cannot be collected otherwise. However, a description of evolution of processes in response to external forcing in the upper layers of the ocean will require coverage by a network of AUVs or other platforms, such as ships, to capture the larger scales; see, e.g., [25].

Doing repeated autonomous missions with AUVs in the Arctic will also prompt the need for more elaborate instrumentation and acoustic navigation infrastructure, mission optimization related to energy conservation and front coverage, risk management, and fault tolerant control. One could also foresee including detection and avoidance of sea ice to ensure a more safe operation.

## VI. CONCLUSION

Operating in harsh environments without human supervision and limited communications is especially important for regions such as the Arctic. In this article, we have presented a method for autonomous adaptive sampling of frontal features, based on a subsumption architecture. The state-based sampling agent uses a classical zigzag maneuver to track the front, as well as featuring the capability to recover tracking if the gradient signature is lost. During field experiments north of Svalbard ( $82^\circ\text{N}$ ), the agent successfully detected and tracked along an Arctic frontal feature close to the sea ice edge for several kilometers, making a total of six crossings while performing vertical profiles in the water column. Measurements yield a detailed volumetric estimate of the frontal feature with high resolution along the frontal zone, which augments ship-based sampling that was run in parallel. The sampling agent revealed cross-frontal structures, both horizontally and vertically, of the complex water mass compositions found north of Svalbard that would not be possible through ship-based sampling only. A deeper understanding of



small-scale processes at frontal systems will improve ecosystem models in these highly productive areas. The AUV is central here as it provides substantial value through efficient and targeted sampling of dynamic processes. However, linking the high-resolution observations to external forcing requires multiplatform sampling strategies (e.g., the use of multiple AUVs, gliders, and a ship that operate simultaneously). The results demonstrate a framework for conducting interdisciplinary oceanographic data collection in the Arctic, combining new technologies to achieve a detailed picture of water-column processes.

#### ACKNOWLEDGMENT

The authors would like to thank the *R/V Kronprins Haakon* crew for the field support and also thank two anonymous reviewers for their critical comments and suggestions that improved the paper.

#### REFERENCES

- [1] I. M. Belkin, P. C. Cornillon, and K. Sherman, "Fronts in large marine ecosystems," *Prog. Oceanogr.*, vol. 81, no. 1–4, pp. 223–236, 2009. [Online]. Available: <http://www.sciencedirect.com/science/article/pii/S0079661109000330>
- [2] J. Le Fèvre, "Aspects of the biology of frontal systems," *Adv. Mar. Biol.*, vol. 23, pp. 163–299, 1987. [Online]. Available: <http://www.sciencedirect.com/science/article/pii/S0065288108601091>
- [3] C. B. Woodson and S. Y. Litvin, "Ocean fronts drive marine fishery production and biogeochemical cycling," *Proc. Nat. Acad. Sci. USA*, vol. 112, no. 6, pp. 1710–1715, 2015.
- [4] P. Munk, C. J. Fox, L. J. Bolle, C. J. G. Van Damme, P. Fossum, and G. Kraus, "Spawning of North Sea fishes linked to hydrographic features," *Fisheries Oceanogr.*, vol. 18, no. 6, pp. 458–469, 2009, doi: [10.1111/j.1365-2419.2009.00525.x](https://doi.org/10.1111/j.1365-2419.2009.00525.x).
- [5] E. D'Asaro, C. Lee, L. Rainville, R. Harcourt, and L. Thomas, "Enhanced turbulence and energy dissipation at ocean fronts," *Science*, vol. 332, no. 6027, pp. 318–322, 2011.
- [6] J. R. Taylor and R. Ferrari, "Ocean fronts trigger high latitude phytoplankton blooms," *Geophys. Res. Lett.*, vol. 38, no. 23, 2011, Art. no. L23601, doi: [10.1029/2011GL049312](https://doi.org/10.1029/2011GL049312).
- [7] Z. Koenig, I. Fer, E. Kolås, T. O. Fossum, P. Norgren, and M. Ludvigsen, "Observations of turbulence at a near-surface temperature front in the Arctic Ocean," *J. Geophys. Res., Oceans*, vol. 125, no. 4, 2020, Art. no. e2019JC015526, doi: [10.1029/2019JC015526](https://doi.org/10.1029/2019JC015526).
- [8] N. E. Leonard, D. A. Paley, F. Lekien, R. Sepulchre, D. M. Fratantoni, and R. E. Davis, "Collective motion, sensor networks, and ocean sampling," *Proc. IEEE*, vol. 95, no. 1, pp. 48–74, Jan. 2007.
- [9] M. L. Seto, *Marine Robot Autonomy*. Berlin, Germany: Springer, 2013.
- [10] S. Frolov, B. Garau, and J. Bellingham, "Can we do better than the grid survey: Optimal synoptic surveys in presence of variable uncertainty and decorrelation scales," *J. Geophys. Res., Oceans*, vol. 119, pp. 5071–5090, 2014.
- [11] J. Das *et al.*, "Data-driven robotic sampling for marine ecosystem monitoring," *Int. J. Robot. Res.*, vol. 34, no. 12, pp. 1435–1452, 2015. [Online]. Available: <http://ijr.sagepub.com/content/34/12/1435.full>
- [12] Y. Zhang, M. A. Godin, J. G. Bellingham, and J. P. Ryan, "Using an autonomous underwater vehicle to track a coastal upwelling front," *IEEE J. Ocean. Eng.*, vol. 37, no. 3, pp. 338–347, Jul. 2012.
- [13] R. N. Smith, F. Py, P. Cooksey, G. Sukhatme, and K. Rajan, "Adaptive path planning for tracking ocean fronts with an autonomous underwater vehicle," in *Proc. Int. Symp. Exp. Robot.*, Jun. 2016, pp. 761–775.
- [14] T. B. Curtin, J. G. Bellingham, J. Catipovic, and D. Webb, "Autonomous oceanographic sampling networks," *Oceanography*, vol. 6, no. 3, pp. 86–94, 1993. [Online]. Available: <http://www.jstor.org/stable/43924649>
- [15] S. R. Ramp *et al.*, "Preparing to predict: The second autonomous ocean sampling network (AOSN-II) experiment in the Monterey Bay," *Deep-Sea Res. II, Top. Stud. Oceanogr.*, vol. 56, no. 3–5, pp. 68–86, 2009.
- [16] E. Carmack *et al.*, "Toward quantifying the increasing role of oceanic heat in sea ice loss in the new Arctic," *Bull. Amer. Meteorol. Soc.*, vol. 96, no. 12, pp. 2079–2105, 2015.
- [17] Y. Zhang *et al.*, "Autonomous front tracking by a wave glider," in *Proc. OCEANS MTS/IEEE Conf.*, Monterey, CA, USA, Sep. 2016, pp. 1–4.
- [18] C. J. Cannell and D. J. Stilwell, "A comparison of two approaches for adaptive sampling of environmental processes using autonomous underwater vehicles," in *Proc. MTS/IEEE OCEANS Conf.*, vol. 2, Sep. 2005, pp. 1514–1521.
- [19] S. Petillo, H. Schmidt, P. Lermusiaux, D. Yoerger, and A. Balasuriya, "Autonomous & adaptive oceanographic front tracking on board autonomous underwater vehicles," in *Proc. OCEANS Conf.*, May 2015, pp. 1–10.
- [20] J. Pinto, R. Mendes, J. C. B. da Silva, J. M. Dias, and J. B. de Sousa, "Multiple autonomous vehicles applied to plume detection and tracking," in *Proc. MTS/IEEE OCEANS Conf., Kobe*, Japan, May 2018, pp. 1–6.
- [21] N. A. Cruz and A. C. Matos, "Reactive AUV motion for thermocline tracking," in *Proc. IEEE OCEANS Conf.*, Sydney, Australia, May 2010, pp. 1–6.
- [22] Y. Zhang *et al.*, "Thermocline tracking based on peak-gradient detection by an autonomous underwater vehicle," in *MTS/IEEE OCEANS Conf.*, Seattle, WA, USA, Sep. 2010, pp. 1–4.
- [23] S. Petillo, A. Balasuriya, and H. Schmidt, "Autonomous adaptive environmental assessment and feature tracking via autonomous underwater vehicles," in *Proc. MTS/IEEE OCEANS Conf.*, Sydney, Australia, May 2010, pp. 1–9.
- [24] N. A. Cruz and A. C. Matos, "Autonomous tracking of a horizontal boundary," in *OCEANS Conf.*, St. John's, NL, Canada Oceans St John's, 2014, pp. 1–6.
- [25] A. Branch *et al.*, "Front delineation and tracking with multiple underwater vehicles," *J. Field Robot.*, vol. 36, no. 3, pp. 568–586, 2019, doi: [10.1002/rob.21853](https://doi.org/10.1002/rob.21853).
- [26] R. Brooks, "A robust layered control system for a mobile robot," *IEEE J. Robot. Autom.*, vol. JRA-2, no. 1, pp. 14–23, Mar. 1986.
- [27] A. Sousa *et al.*, "LAUV: The man-portable autonomous underwater vehicle," in *Proc. IFAC Workshop Nav., Guid., Control Underwater Veh.*, vol. 3, 2012, pp. 268–274.
- [28] J. Pinto *et al.*, "Implementation of a control architecture for networked vehicle systems," *IFAC Proc. Vol.*, vol. 45, no. 5, pp. 100–105, 2012.
- [29] J. Pinto, P. S. Diasand, R. Martins, J. Fortuna, E. Marques, and J. Sousa, "The LSTS toolchain for networked vehicle systems," in *MTS/IEEE OCEANS Conf.*, 2013, pp. 1–9.
- [30] F. Py, K. Rajan, and C. McGann, "A systematic agent framework for situated autonomous systems," in *Proc. 9th Int. Conf. Auton. Agents Multiagent Syst.*, May 2010, pp. 583–590.
- [31] K. Rajan and F. Py, "T-REX: Partitioned inference for AUV mission control," in *Further Advances in Unmanned Marine Vehicles*, G. N. Roberts and R. Sutton, Eds. London, U.K.: IET, Aug. 2012.
- [32] N. A. C. Cressie and C. K. Wike, *Statistics for Spatio-Temporal Data (Wiley Series in Probability and Statistics)*. Hoboken, NJ, USA: Wiley, 2011.
- [33] R. Graham, F. Py, J. Das, D. Lucas, T. Maughan, and K. Rajan, "Exploring space-time tradeoffs in autonomous sampling for marine robotics," in *Experimental Robotics*. Berlin, Germany: Springer, 2013, vol. 88, pp. 819–839. [Online]. Available: <http://link.springer.com/10.1007/978-3-319-00065-7>
- [34] J. Eidsvik, T. Mukerji, and D. Bhattacharjya, *Value of Information in the Earth Sciences: Integrating Spatial Modeling and Decision Analysis*. Cambridge, U.K.: Cambridge Univ. Press, 2015. [Online]. Available: <https://www.cambridge.org/core/books/value-of-information-in-the-earth-sciences/61119AB2F707D557E49E00BF9FD6FE39>
- [35] T. O. Fossum *et al.*, "Information-driven robotic sampling in the coastal ocean," *J. Field Robot.*, vol. 35, no. 7, pp. 1101–1121, 2018. [Online]. Available: <https://onlinelibrary.wiley.com/doi/abs/10.1002/rob.21805>
- [36] T. O. Fossum, C. Travelletti, J. Eidsvik, D. Ginsbourger, and K. Rajan, "Learning excursion sets of vector-valued Gaussian random fields for autonomous ocean sampling," *Ann. Appl. Statist.*, 2021. [Online]. Available: <https://imstat.org/journals-and-publications/annals-of-applied-statistics/annals-of-applied-statistics-next-issues/>



**Trygve Olav Fossum** received the M.Sc. and Ph.D. degrees in marine robotics from the Norwegian University of Science and Technology (NTNU), Trondheim, Norway, in 2008 and 2018, respectively.

He is currently a Researcher with the Applied Underwater Robotics Laboratory, NTNU. In 2018, he was a Visiting Researcher with Monterey Bay Aquarium Research Institute, Moss Landing, CA, USA. He leads the company Skarv Technologies, which he founded in 2019, a company focusing on industrial underwater autonomy solutions. His current research

interests include effective data collection strategies using unmanned underwater vehicles, applied machine intelligence, and planning algorithms.



**Frank Nilsen** received the Ph.D. degree in physical oceanography from the Geophysical Institute, University of Bergen, Bergen, Norway, in 2001.

He is currently a Professor in Physical Oceanography with the University Centre in Svalbard (UNIS), Longyearbyen, Svalbard and Jan Mayen, and the University of Bergen. During the International Polar Years from 2007 to 2010, he was leading the measurements programs on sea ice freezing in Storfjorden and heat loss in the West Spitsbergen Current and how warm water is able to penetrate the Arctic fjords and melt the sea ice during winter. Lately, the ocean current dynamics north of Svalbard along the Nansen basin and the coupling to the northern Barents Sea have become the main focus through the big national project the Nansen Legacy. His research interests include air–ice–sea interaction and processes that contribute to the cooling of the warm Atlantic water flowing along the continental shelf of Svalbard toward the Arctic Ocean. Svalbard is a unique laboratory for studying sea ice freezing and melting processes.



**Petter Norgren** received the M.Sc. degree in engineering cybernetics and the Ph.D. degree in marine cybernetics from the Norwegian University of Science and Technology (NTNU), Trondheim, Norway, in 2011 and 2018, respectively.

From 2012 to 2013, he was with Marine Cybernetics AS involved in hardware in-the-loop testing of marine control systems. Since 2018, he has been a Postdoctoral Fellow with NTNU, involved in the Nansen Legacy program. In 2019, he cofounded Skarv Technologies, a company focusing on industrial underwater autonomy solutions, where he is currently a Chief Technology Officer. His research interests include AUVs for arctic marine operations and research, simultaneous localization and mapping, autonomous exploration, and tracking and monitoring of AUVs using USVs.



**Ilker Fer** received the Ph.D. degree in lake hydrodynamics from the Swiss Federal Institute of Technology Lausanne, Lausanne, Switzerland, in 2001.

He is currently a Professor of Physical Oceanography with Geophysical Institute, University of Bergen, Bergen, Norway. He is the leader of the research infrastructure “the Norwegian Node for the European Multidisciplinary Seafloor and Water Column Observatory” and “Norwegian National Facility for Ocean Gliders.” He is an Observational Oceanographer with field experience at sea and on ice, and has led more

than 25 expeditions since 2000. He has expertise in collecting, processing, and analyzing data from conventional ship and moored instruments, as well as from various complex platforms including microstructure profilers, gliders, moored profilers, and eddy-covariance systems. His research interests include meso to small-scale processes in physical oceanography with special attention to high-latitudes, ocean mixing and turbulence, and atmosphere–ocean–ice interaction.



**Zoe Charlotte Koenig** (Member, IEEE) received the M.Sc. degree in oceanography at Ecole Normal Supérieure, Paris, France and the Ph.D. degree from University Pierre and Marie Curie, Paris, France, in 2017.

She is currently a Postdoc Researcher within the Nansen Legacy Project, University of Bergen, Bergen, Norway, and the Norwegian Polar Institute. She is also a Physical Oceanographer. She is currently working on the ocean dynamics in the Barents Sea and north of Svalbard from *in situ* observations.



**Martin Ludvigsen** received the M.Sc. degree in engineering cybernetics and the Ph.D. degree in marine cybernetics from the Norwegian University of Science and Technology (NTNU), Trondheim, Norway, in 2011 and 2018, respectively.

He is currently a Professor with the Department of Marine Technology and works with underwater vehicles and robotics. He is also a Manager for the Applied Underwater Laboratory (AURLab), Norwegian University of Science and Technology (NTNU), Trondheim, Norway. AUR-Lab is an asset for multidisciplinary marine research with NTNU, facilitating research within both engineering disciplines and marine science. He is also a cofounder of Blueye Robotics, a novel portable ROV start-up. He has an extensive at-sea experience in Arctic waters as well as in benthic environments associated with the Norwegian mid-ocean ridge. He has been involved in a variety of research projects both on deep sea research in the upper water column and in the Arctic deploying robotic underwater vehicles. He holds a position as an Adjunct Associate Professor in marine technology with the Svalbard University Centre (UNIS), Longyearbyen. He is currently an affiliated Scientist with the Centre for Autonomous Marine Operations and Systems (NTNU AMOS).